THE JOURNAL OF PHYSICAL CHEMISTRY A
A JOURNAL OF THE AMERICAN CHEMICAL SOCIETY

pubs.acs.org/JPCA

Article

Blue-Shifted and Broadened Fluorescence Enhancement by Visible and Mode-Selective Infrared Double Excitations

Published as part of The Journal of Physical Chemistry A virtual special issue "Xueming Yang Festschrift".

Qirui Yu, Xinmao Li, Chengzhen Shen, Zhihao Yu, Jianxin Guan,* and Junrong Zheng*

Cite This: *J. Phys. Chem. A* 2024, 128, 2912−2922

Read Online

ACCESS | Metrics & More | Article Recommendations | Supporting Information

ABSTRACT: Mode-selective vibrational excitations to modify the electronic states of fluorescein dianion in methanol solutions are carried out with a femtosecond visible pulse synchronized with a tunable high-power, narrow-band picosecond infrared (IR) pulse. In this work, simultaneous intensity enhancement, peak blueshift, and line width broadening of fluorescence are observed in the visible/IR double resonance experiments. Comprehensive investigations on the modulation mechanism with scanning the vibrational excitation frequencies, tuning the time delay between the two excitation pulses, theoretical calculations, and nonlinear and linear spectroscopic measurements suggest that the fluorescence intensity enhancement is caused by the increase of the Franck−Condon factor induced by the vibrational excitations at the electronic ground state. Various enhancement effects are observed as vibrations initially excited by the IR photons relax to populate the vibrational modes of lower frequencies. The peak blueshift and line width broadening are caused by both increasing the Franck−Condon factors among different subensembles because of IR pre-excitation and the long-lived processes induced by the initial IR excitation. The results demonstrate that the fluorescence from the visible/IR double resonance experiments is not a simple sum frequency effect, and vibrational relaxations can produce profound effects modifying luminescence.

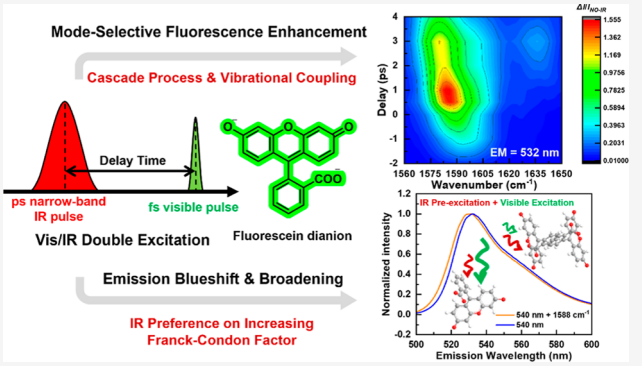

1. INTRODUCTION

Luminescence, one of the ubiquitous phenomena in nature resulting from the relaxation of electronic excited states, plays crucial roles in many research areas. Modulation of molecular luminescent properties has long been a central topic in a wide range of research and practical applications, e.g., biosensing and light-emitting devices.[1−11] Luminescence can be modulated by chemical or physical methods. Chemical methods include directly modifying molecular structures such as replacing the functional groups and adjusting the conjugation extent,[12−16] changing the chemical environments, e.g., solvent polarity, pH, or temperature,[17−21] and altering the physical states, e.g., aggregation-induced quenching and aggregation-induced emission.[22−25]

Physical methods, usually optical manipulations, are also often used to modulate the fluorescence. For instance, the two-photon fluorescence using two near-infrared pulses to produce fluorescence to avoid sample damage caused by direct absorption of visible photons.[26,27] Continuous and pulsed mid-infrared lights are also applied to modulate fluorescence by exciting molecular vibrations.[28−41] Very recently, a femtosecond (fs) visible and mid-IR double resonance approach[42] and a picosecond (ps) visible and mid-IR double resonance approach[43] have been able to, respectively, achieve single-molecule sensitivity with chemical bond information encoded in fluorescence, opening a new avenue for fluorescence modulation.

The visible/mid-IR double resonance method is a two-photon experiment in which both the vibrational and electronic states are simultaneously excited. Different from the typical near-infrared two-photon fluorescence methods, a high-frequency vibrational excitation can induce or alter various molecular transformations at an electronic excited state, e.g., energy relaxations, electronic transfers, and molecular structural evolutions,[44−57] modifying both the nonradiative and radiative decays of the electronic excited state. Therefore, the effect of the visible/mid-IR double resonance is not a simple sum frequency. The luminescence from the double resonance can differ significantly from that of

Received: October 25, 2023
Revised: March 22, 2024
Accepted: March 25, 2024
Published: April 4, 2024

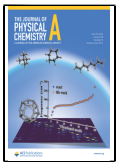

https://doi.org/10.1021/acs.jpca.3c07060
J. Phys. Chem. A 2024, 128, 2912−2922

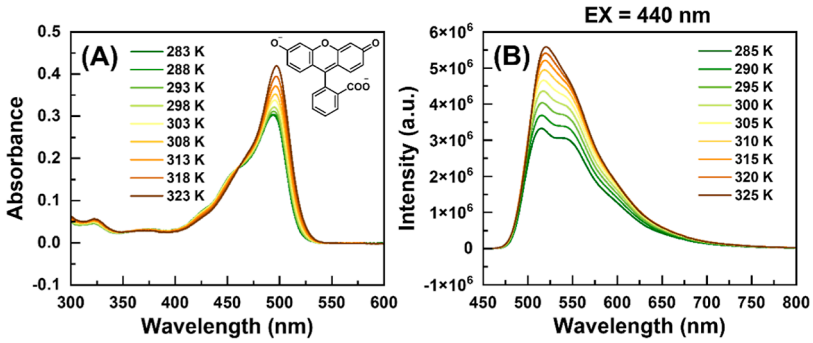

Figure 1. UV−visible absorption spectra and luminescence spectra by 440 nm excitation of 10^{-5} M methanol solution of fluorescein dianion (deprotonated by NaOH) at different temperatures. The molecular structure of fluorescein dianion is displayed as the inset in Figure 1A.

direct excitation by a single photon, which is yet to be explored.

In this work, we aim to investigate the influence of mode-specific vibrational excitations on the fluorescence behavior of visible/mid-IR double resonance experiments. A combination of ps high-power mid-IR pulse and fs UV−visible pulse is applied in the experiments, different from previous works either using double fs or ps beams.[42,43] The time delay of the two pulses is controlled by a delay line. The fs/ps approach provides sufficiently high vibrational excitation power by the ps IR pulse to generate a significantly large number of double excited molecules (compared to that only excited by the UV−visible photon) and an excellent temporal resolution by the fs UV−visible pulse.[58] Both are important to obtain mode-selective vibrational relaxation and time-delay-dependent frequency-resolved fluorescence with an excellent signal-to-noise ratio.

Methanol solutions of fluorescein dianion are chosen as model systems in this study. Fluorescein is one of the most common fluorescent probes. It has a very large absorption coefficient ε of 76,900 M^{-1} cm^{-1} at 490 nm and a fluorescence quantum yield of > 90% in water solvent.[17,59] Both factors contribute to its extremely high sensitivity as a fluorescent sensing chromophore. The temperature-dependent UV−visible and fluorescence spectra of a fluorescein dianion solution are displayed in Figure 1. In a condensed solution with a protic solvent, fluorescein dianion molecules tend to aggregate to form dimers.[59,60] As temperature rises, the monomer/dimer equilibrium shifts to more monomers, resulting in the increase of absorbance at 490 nm as displayed in Figure 1A and fluorescence intensity enhancement and redshift as displayed in Figure 1B. The excitation wavelength for the fluorescence spectra displayed in Figure 1B is 440 nm, which is far away from the maximum absorption of monomer at 490 nm but closer to the absorption peaks of dimer at 460 and 428 nm. Thus, the photons at 440 nm probably prefer to excite dimers. It is interesting to note that the fluorescence line shape is dependent on the excitation wavelength and the sample concentration because of factors like the existence of different species, e.g., monomer and dimer, and self-absorption. In the ultrafast experiments, the concentration of 0.01 M is selected to guarantee an acceptable monomer/dimer ratio (~8% of monomer aggregates to dimer[61]) and nonlinear spectral signal-to-noise ratio. The fluorescence spectra used in the comparison with ultrafast data are collected with the same concentration and excited with wavelengths (540, 490, and 500 nm) that are relevant to the ultrafast experimental conditions.

2. METHODS

2.1. Experimental Setup. The ultrafast measurements are conducted with a home-built system briefly introduced as follows. Details of the measurements with routine techniques are provided in the SI.

2.1.1. Ultrafast Spectroscopy. The Vis-pump/IR-probe spectroscopic studies are performed according to a pervious report.[62] Briefly, laser pulses (1 kHz, ~ 40 fs pulse width, 800 nm central wavelength) from an amplified Ti/sapphire laser system (UpTek Solutions Inc.) are split into two parts. One is used to pump a femtosecond optical parametric amplifier (OPA) (TOPAS-Prime), producing ~60 fs UV/visible pulses with a bandwidth of ~10 nm in a tunable frequency ranging from 250 to 800 nm at 1 kHz. The other is used to pump another fs OPA (Palitra, QUANTRONIX), producing mid-IR pulses with a bandwidth ~200 cm^{-1} in a tunable frequency range from 1000 to 3500 cm^{-1} at 1 kHz. The visible beam excites the electron transition, and the excitation power is ~200 μW with a spot diameter of 245 μm. The mid-IR beam is used as the probe beam and collected by a 2 × 64 pixel mercury cadmium telluride (MCT) detector (Infrared Associates) with a spectral resolution of ~3 cm^{-1}. Two polarizers are inserted into the mid-IR beam path. One is located behind the sample to selectively measure the parallel or vertical polarized signal relative to the pump beam, and another is before the sample, which is used to rotate the polarization of the probe beam about 45° relative to that of the pump beam. Measuring the transmission of the mid-IR beam through the sample by chopping the pump beam at 500 Hz, the pump−probe signal $P(t)$ is collected, and the vibrational lifetimes are obtained from the rotation-free signal $P(t) = (P_{\parallel}(t) + 2P_{\perp}(t))/3$, and anisotropy $A(t)$ is calculated from the following equation

$$A(t) = (P_{\parallel}(t) - P_{\perp}(t))/(P_{\parallel}(t) + 2P_{\perp}(t)) \quad (1)$$

where $P_{\parallel}(t)$ and $P_{\perp}(t)$ are the parallel and vertical signals, respectively.

The IR-pump/probe studies are performed with a fs/ps synchronized laser system.[63] The fs laser is described as above, and its mid-IR output serves as the probe beam. The output (1 kHz, ~ 1.5 ps pulse width, 800 nm central wavelength) from a ps amplified Ti/sapphire laser system (UpTek Solutions Inc.) is used to pump a ps OPA (TOPAS-Prime) producing ~1−2 ps IR pulses with a bandwidth of ~10−20 cm^{-1} in the range from 900 to 3600 cm^{-1}, serving as the pump beam.

2.1.2. Visible/IR Double Resonance Fluorescence Experiment. Briefly, the fs visible beam spatially overlaps with the ps

https://doi.org/10.1021/acs.jpca.3c07060
J. Phys. Chem. A 2024, 128, 2912−2922

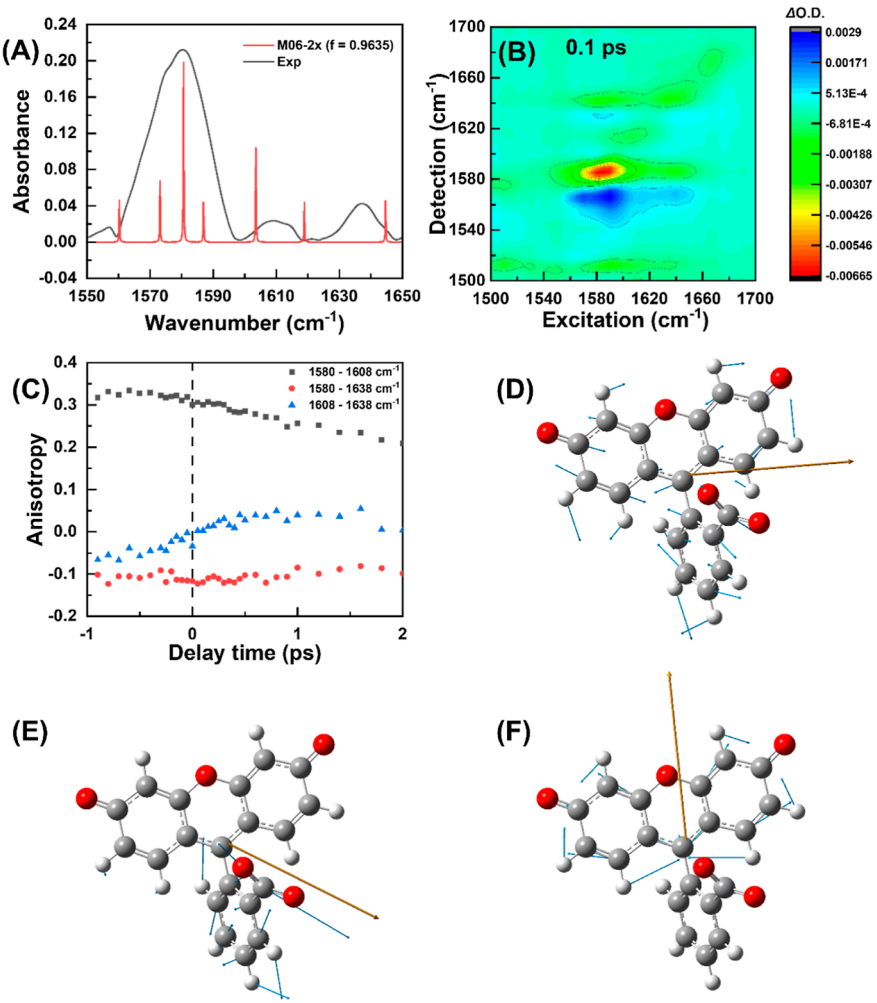

Figure 2. (A) Comparison of experimental and calculated IR spectra of the sample in the double resonance experiments; (B) 2D-IR spectrum of the sample at 0.1 ps delay time; (C) 2D-IR signal anisotropy decay of the off-diagonal peaks belonging to 1580/1608 cm^{-1} (black), 1580/1638 cm^{-1} (red), and 1608/1638 cm^{-1} (blue). (D–F) Vibrational modes and dipole moment derivatives of (D) 1580 cm^{-1}, (E) 1608 cm^{-1}, and (F) 1637 cm^{-1}. Gold arrows represent the mode 0–1 transition dipole moment directions.

IR pulse on the sample. The time delay between visible and ps-IR pulses is controlled with a delay line. The wavelength-resolved fluorescence is collected by an objective lens into an optical fiber and sent to a spectrograph (Shamrock SR303i) equipped with an EMCCD instrument (Newton EM, Andor DU970). With a visible excitation power of 10 μW, the integral time is about 50 s.

2.2. Results and Discussion. *2.2.1. Vibrational Mode Assignments.* The Fourier transform infrared (FTIR) spectrum of a 10^{-2} M fluorescein dianion methanol solution is displayed in Figure 2A, as well as the calculated spectrum (Figure S1). In the range from 1550 to 1650 cm^{-1}, three major peaks at 1580, 1608, and 1637 cm^{-1} peaks are identified. By frequency scaling, theses peaks match well with the strong skeleton stretch (Figure 2D), the benzoic carboxyl stretch (Figure 2E), and the xanthene skeleton stretch whose dipole derivative is parallel to the C–C bond, which connects the xanthene ring and benzoic ring (abbreviated as P) (Figure 2F), respectively.

To further confirm the assignments of these modes, 2D-IR experiments are carried out. A 2D-IR spectrum at a waiting time of 0.1 ps is displayed in Figure 2B. Cross peaks appear at 1580, 1608, and 1638 cm^{-1}, indicating that these modes are coupled. The vibrational cross angle $\theta(t)$ between two modes can be obtained from the anisotropy

$$A(t) = (3\cos^2\theta(t) - 1)/5 \quad (2)$$

where $\theta(0)$ represents the inherent angle between two infrared transition dipole moments. As displayed in Figure 2C, the experimental initial anisotropy $A(0)$ of 1580/1608, 1580/1638, and 1608/1638 cm^{-1} are 0.30, −0.12, and 0.00, respectively, which are close to the theoretical calculation results of 0.25, −0.20, and −0.04. The results support the peak assignments. The peak located at 1621 cm^{-1} between 1608 and 1637 cm^{-1} represents benzoic ring stretch (Figure S1D). The peak located at 1575 cm^{-1} is the xanthene skeleton stretch of which the dipole derivative is vertical to the C–C bond, which connects the xanthene ring and benzoic ring (abbreviated as V) (Figure S1E). It is also likely that a weak skeleton stretch peak hides within the huge absorption peak between 1580 and 1598 cm^{-1} (Figure S1F).

2.2.2. Visible/IR Double Resonance Enhances and Blue-Shifts Fluorescence. When excited at the red edge of the absorption with the fs pulse centered at 540 nm, the sample fluoresces weakly and peaks at 532.5 nm (Figure 3A). With a simultaneous ps IR pulse added on, the fluorescencece

https://doi.org/10.1021/acs.jpca.3c07060
J. Phys. Chem. A 2024, 128, 2912–2922

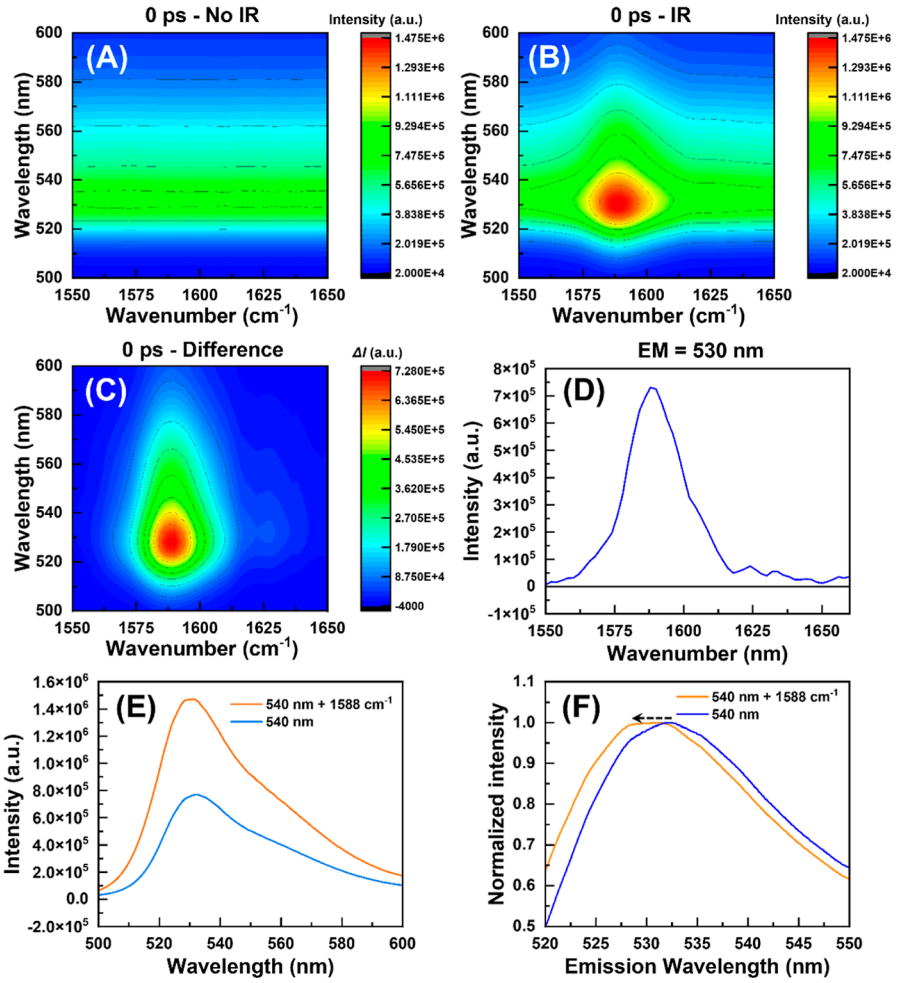

Figure 3. Fluorescence emission spectra excited with fs 540 nm visible photons (A) without and (B) with ps IR modulation by simultaneous excitation. (C) Difference spectrum of (A) subtracted from (B). (D) Infrared resolved fluorescence enhancement spectrum at the emission wavelength of 530 nm extracted from (C). (E,F) Fluorescence spectra excited at 1588 cm^{-1} extracted from (A,B), illustrating the enhancement (E) and the blueshift (F), respectively.

intensity increases and reaches more than two times at 1588 cm^{-1} (Figure 3B–E), close to the FTIR peak of the strong skeleton stretch. At 1606, 1628, and 1638 cm^{-1}, various degrees of modulations appear as well (Figure 3D). The emission peak also blue-shifts for 2.5 nm from 532.5 to 530 nm.

On the one hand, as suggested by previous works,[42,43] the IR/visible double resonance effectively promotes the electronic transition from the vibrational excited state rather than the vibrational ground state of the electronic ground state, resulting in the electronic transition gap equal to the sum frequency of the two excitation photons. In the experiments discussed above, the visible excitation wavelength is 540 nm, at the red edge of absorption, where only a very small fraction of molecules are visible-excited (see Supporting Information Part 12). Summing the IR pulse of 1588 cm^{-1} with it leads to a photonic wavelength of 497 nm, very close to the absorption center. This implies that the molecules in the vibrational excited state have a much larger cross-section absorbing the 540 nm photons than those in the vibrational ground state. Therefore, the probability of absorbing visible photons by these vibrationally excited molecules will be much larger than that by the rest of the molecules at the vibrational ground state. In other words, the vibrational excitation must increase the absorption of the visible photons and, thus, the number of molecules at the electronic excited state. As a result, a greater emission enhancement is naturally expected in the double resonance experiment. The enhancement is observed, as displayed in Figure 3. In fact, the absorption of 540 nm light also increased substantially, induced by the vibrational excitation at 1588 cm^{-1} (Figure S6). The different enhancement effects by IR excitation in Figure 3D look to be correlated to the absorbance at various wavenumbers. However, it seems that the maximum enhancement effect located at 1588 cm^{-1} in Figure 3D does not belong to any vibrational modes, and the enhancement effects of other vibrational modes are not proportional to the absorbance in the FTIR spectrum. This issue will be discussed later.

On the other hand, with the existence of the aggregates, the fluorescence emission is excitation-wavelength-dependent (Figure 6E), making it not so straightforward to analyze the origin of blueshift and line width. In the following paragraphs, this observation is discussed with more experimental evidence.

2.2.3. Cascade Decay with Time Delay and Shifts of Modulation Peaks Are Observed from Time-dependent Double Excitation. Time-delay-dependent experiments are performed to further investigate the double-resonance-induced emission. The time delay is the interval between the infrared

https://doi.org/10.1021/acs.jpca.3c07060
J. Phys. Chem. A 2024, 128, 2912–2922

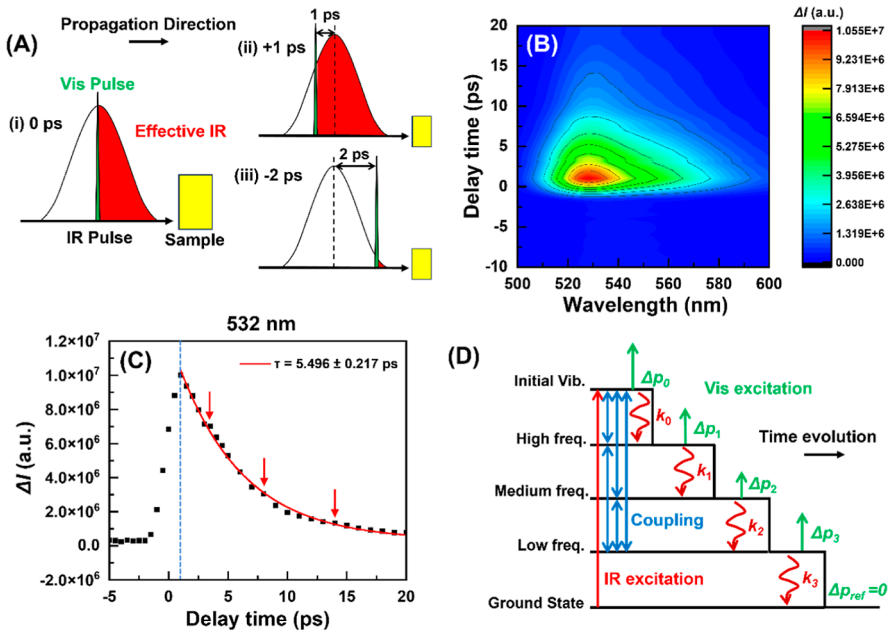

Figure 4. (A) Time sequence of the experiments. The visible pulse arriving earlier is defined as the negative time, and the positive time refers to the infrared pulse arriving earlier. The scheme illustrates the effective IR excitation at delay time of (i) 0 ps; (ii) 1 ps; (iii) −2 ps as light propagates from left to right. (B) Time dependence of fluorescence enhancement by double resonance excited with a 540 nm visible fs laser and a 1585 cm^{-1} infrared ps pulse. (C) The evolution of fluorescence enhancement is observed at the emission wavelength of 532 nm. The dashed line shows that the maximum appears at about 1 ps. The arrows indicate intensity oscillations. (D) Cascade vibrational relaxation and the coupling process. Molecules are first excited by infrared pulses (bright red) and relax to different dark modes from higher vibrational energy to lower by multisteps with rate constants k_i as delay time evolves (dark red). On each dark mode, the possibility of absorbing visible photons (green) is increased by Δp_i in varying degrees comparing to that in the vibrational ground state, and Δp_{ref} equals to 0 as the reference. Different vibrational modes are also possible to couple to each other as time evolves.

pulse and the visible pulse. The visible pulse arriving earlier is defined as the negative time, and the positive time refers to the infrared pulse arriving earlier (Figure 4A). Figure 4B displays the time dependence of fluorescence enhancement by double resonance excited with a 540 nm visible fs laser and a 1585 cm^{-1} infrared ps pulse. The evolution of the fluorescence enhancement at the emission wavelength of 532 nm is plotted in Figure 4B. Several interesting features appear.

First, before time zero, the fluorescence is slightly enhanced, as confirmed by the positive nonzero signal before time zero in Figure 4C, and the effect starts to increase rapidly at −2 ps. The slightly enhanced fluorescence before −2 ps is red-shifted and its line width are broadened, which are similar to fluorescence spectra at higher temperatures (Figures 6D and S8C,D). Therefore, it is very likely that the vibrational excitation relaxes and produces a local heat effect, slightly increasing the temperature so that the fluorescence behaves like that at a higher temperature.

Second, the overall decay time constant in Figure 4C is 5.5 ps, which is close to the time constant ∼5.0 ps of vibrational relaxation at 1585 cm^{-1} (Figure S5B), indicating the effective mode at 1585 cm^{-1} which enhances the fluorescence are short-lived. The maximum emission occurring at 1 ps instead of time zero is the result of signal convolution, as shown in Figure 4A.

Third, except for an exponential decay process of fluorescence enhancement, sudden emission intensity jumps appear at 3, 7, and 14 ps and decay differently (the dots pointed by arrows in Figure 4B). The jumps are not oscillations caused by coupled vibrations excited by the IR pulse as they do not appear in the IR pump probe data (Figures S5B,S11C). The observed enhancement oscillation phenomenon can be understood in terms of the general vibrational relaxation mechanism. The relaxation of a high-frequency vibrational mode is typically a cascade process.[64−66] It can relax to populate the vibrational modes of medium frequencies, which in turn can further relax to populate modes of lower frequencies and so on through coupling mediated by a solvent−solute interaction. These intermediate modes can also result in fluorescence enhancement if they have relatively strong electron-vibrational coupling and an effect for Franck−Condon factor enhancement. Besides, the simultaneous excitations of two or more of these low-frequency modes can better increase the Franck−Condon factor (Figure 5F), compared to that with only one mode excited. The scheme of cascade relaxations and vibrational coupling is illustrated in Figure 4D.

More time-dependent experiments are carried out. Vibrational excitation frequencies for fluorescence enhancement are scanned from 1550 to 1650 cm^{-1} at various time delays. Figure 5A−C displays the emission spectra of visible/IR double resonance experiments at different delay times and excited with different IR frequencies. The visible excitation wavelength is 540 nm. At −2 ps (Figure 5A), the maximum enhancement occurs at 1598 cm^{-1}, with other effective wavenumbers at 1584, 1610, and 1630 cm^{-1}. The effective wavenumbers vary to 1584, 1604, and 1626 cm^{-1} at 1 ps (Figure 5B), then 1580, 1608, and 1636 cm^{-1} at 3 ps (Figure 5C), where the enhancement peaks shift to meet with absorption peaks in the FTIR spectrum. These trends can be clearly seen in Figure 5D, where the time dependence of the emission intensity at the emission wavelength of 532 nm is plotted against the IR excitation frequency. The optimal vibrational frequency that

https://doi.org/10.1021/acs.jpca.3c07060
J. Phys. Chem. A 2024, 128, 2912−2922

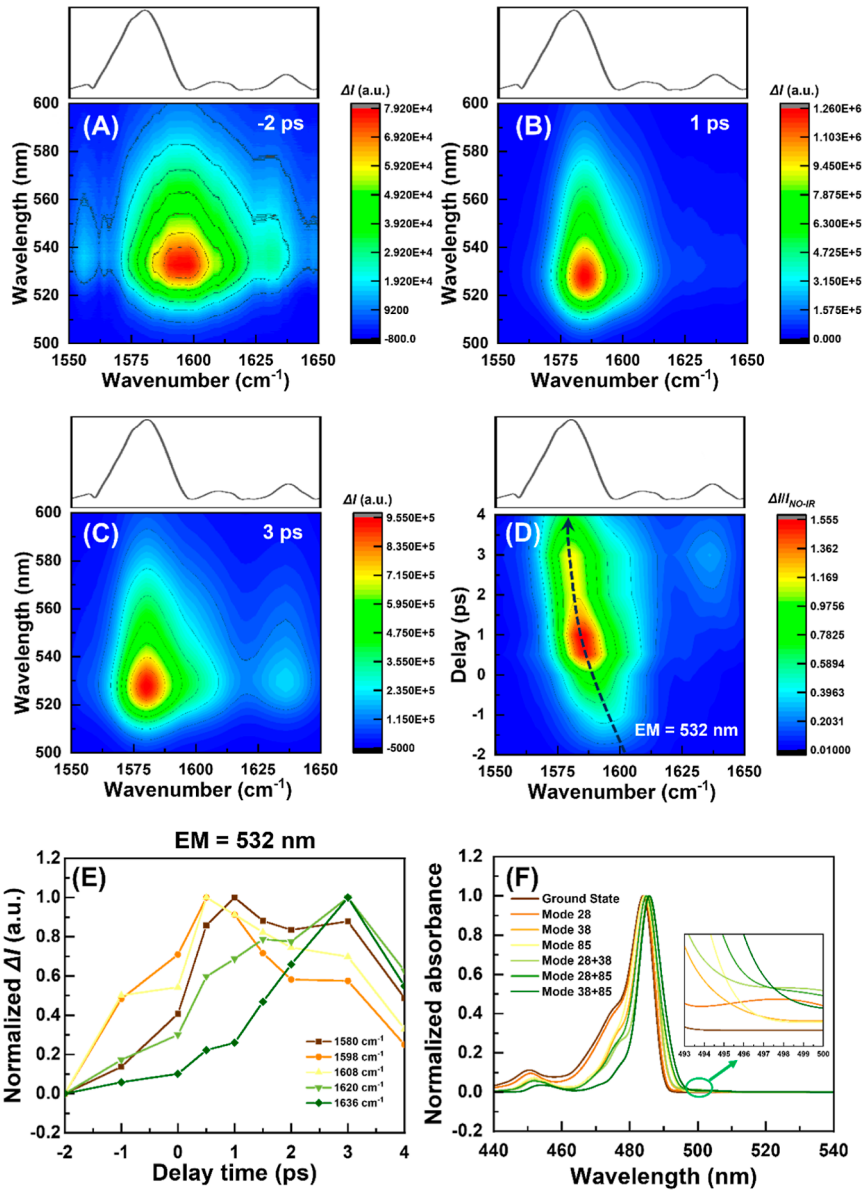

Figure 5. Dynamics of vibrational mode-selective fluorescence enhancement of excited fluorescein manipulation. (A−C) Time evolution of normalized IR-modulated fluorescence spectra compared with that of the FTIR spectrum at −2, 1, and 3 ps, respectively. The optimal vibrational excitation frequency varies with the time delay between the visible and the mid-IR pulses. Full spectra are shown in Figure S7. (D) The time dependence of emission intensity at the emission wavelength of 532 nm is compared to that of the IR excitation frequency. With the IR pulse arriving earlier, the optimal vibrational excitation frequency shifts to a lower frequency, and at 3 ps, the excitation with 1638 cm^{-1} can also produce significant emission enhancement. (E) Normalized time-dependent intensity enhancement spectra by different modulation infrared wavenumbers, extracted from Figure 5D. The maximum intensity emerges at various time delays depending on the initial excited modes. (F) Calculated normalized electronic absorption spectra by IR excitation. Comparing to no IR excitation (dark red), dark modes 28 (orange, the index is matched from low wavenumbers to high) and 38 (yellow) as well as mode 85 (the strong skeleton stretch at 1580 cm^{-1}) can enhance absorbance at the red-edge side effectively. Simultaneous excitations of two vibrational modes lead to better enhancement. More details are shown in Figure S2D.

produces the largest fluorescence enhancement red-shifts tremendously from 1598 cm^{-1} at −2 ps to 1584 cm^{-1} at 1 ps, then 1580 cm^{-1} at 3 ps (dashed line), at which the excitation at 1638 cm^{-1} also reaches its maximum enhancement effect.

Before investigating what causes the optimal modulation wavenumber shifts as time evolves, it is necessary to know how the enhancement effect reaches a maximum at various delay times as different vibrational modes are excited. The detector used in the experiments is EMCCD, of which the signal integration time is much longer than the molecular dynamics time scale involved, meaning that the fluorescence enhancement is a result of accumulation from the entire excitation−relaxation process. Moreover, the ps-IR pulses have a spectral width of 10−20 cm^{-1}, which means that a pulse might simultaneously excite vibrations within this range. Thus, the observed wavenumber-dependent enhancement peaks may be contributed by more than one mode. According to the calculations, 5 modes ranging from 1580 to 1637 cm^{-1} are identified. The frequencies of these modes are 1580 cm^{-1} (mode I, strong skeleton stretch), 1598 cm^{-1} (II, weak skeleton stretch), 1608 cm^{-1} (III, benzoic carboxyl stretch),

https://doi.org/10.1021/acs.jpca.3c07060
J. Phys. Chem. A 2024, 128, 2912−2922

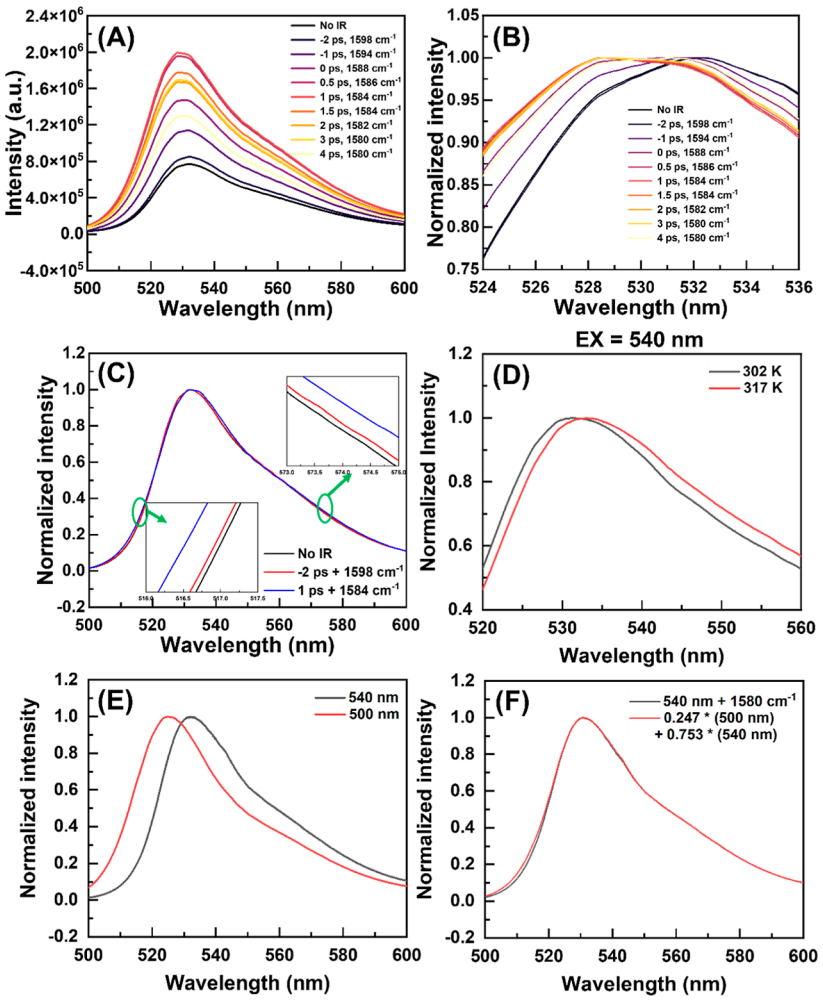

Figure 6. (A,B) Fluorescence emission spectra and normalized spectra with and without optimal IR excitations, extracted from Figure S7. (C) Normalized fluorescence spectra excited with 540 nm fs light (black), 540 nm fs light 2 ps prior to 1598 cm^{-1} excitation (red), and 540 nm fs light 1 ps behind 1584 cm^{-1} excitation (blue, the peak is red-shifted for 3 nm along the *x*-axis for visual aid to compare the line widths). The insets are the enlarged figures at about one-third of the peak height, showing that the blue peak has a larger width than that of the red peak which is wider than the black peak. (D) Normalized fluorescence emission spectra by 540 nm excitation at 302 and 317 K, unambiguously illustrating that the fluorescence red-shifts at a higher temperature. (E) Normalized fluorescence emission spectra by 540 and 500 nm excitation. (F) The overlapping of two spectra in (E) excellently coincides with emission spectra from the visible/IR double resonance. The coefficients of normalized spectra are 0.247 (from 500 nm excitation) and 0.753 (from 540 nm excitation) when the fluorescence intensity increases by 70%.

1621 cm^{-1} (IV, benzoic ring stretch), and 1637 cm^{-1} (V, xanthene skeleton stretch P).

Time-dependent intensity enhancement spectra at these five excitation frequencies are shown in Figure 5E. It is apparent that the time dependence varies with the vibrational frequency. A natural thought is that the vibrations with shorter lifetimes relax and dissipate faster, convoluting with the IR pulse, resulting in the maximum modulation effect emerging earlier for short-lived modes. If so, from Figure 5E, one would expect modes (II) and (III) to have relatively short lifetimes, followed by (I), and modes (IV) and (V) are long-lived. However, the lifetimes of modes (I), (III), and (V) obtained from IR pump/IR probe experiments are 5.0, 2.1, and 2.8 ps, respectively (Figure S5B−D), where (I) is longer-lived than (III), but also than (V). This apparent inconsistency can be understood in terms of the vibrational cascade relaxation or coupling process. Data displayed in Figure 4C already demonstrate that the relaxation of vibrational mode originally excited by 1585 cm^{-1} is a cascade process during which different dark modes have different Franck−Condon factor enhancement. It is very likely the case for excitations at other vibrational frequencies: the initially excited vibration is not necessarily the mode with the largest enhancement factor. The largest enhancement factor can appear in dark modes that are populated by relaxation later. Therefore, the time dependence of fluorescence enhancement is not solely dependent on the lifetime of the initially excited vibration.

Similarly, the vibrational-frequency-dependent fluorescence enhancement in Figure 5D can also be explained in terms of the cascade relaxation or coupling process in Figure 4D. Different vibrational excitations relax to different dark modes with various Franck−Condon factor enhancements at different delays, resulting in a time-dependent vibrational frequency shift. The time-dependent continuous redshift of 18 cm^{-1} in Figure 5D, involving two vibrational modes at least, is more likely a coincidence rather than a necessity.

It would be very interesting to see what the dark modes that enhance the Franck−Condon factor are. Based on the method previously reported,[67] the enhancement of the Franck−Condon factor by vibrational excitations is calculated. The

https://doi.org/10.1021/acs.jpca.3c07060
J. Phys. Chem. A 2024, 128, 2912−2922

results show that double excitations of low-frequency dark modes can better enhance the Franck−Condon factor at the absorption red-edge side than that at the initially IR-excited vibrational modes, whereas a single dark mode is often not so effective (Figure 5F). The result illustrates that a better modulation effect after relaxation is probably contributed by multiple dark modes. Two possible candidates for these dark modes are the skeleton ring stretch located at 578 cm^{-1} (Mode 28 by index, Figure S2E) and the benzoic ring wagging at 728 cm^{-1} (Mode 38, Figure S2F). These modes are coupled to the vibrational modes initially excited in the double resonance experiments and have significant enhancement effects on the Franck−Condon factor, especially when they are simultaneously excited (Figure 5F).

2.2.4. Blue-Shifted and Broadened Fluorescence Emission by Mid-IR Modulation. Besides fluorescence enhancement, the double resonance experiments with different vibrational excitations also produce fluorescence blueshifts compared to that excited only by the 540 nm visible photon, shown in Figure 6A,B. The bluest emission wavelength reaches 529 nm at 1 ps excited by 1584 cm^{-1}, about 3.5 nm on the blue side of the fluorescence peak excited by 540 nm light.

One of the most obvious explanations for the blueshift is that the vibrational excitation makes species that can absorb higher-energy visible photons excited more (resemble the sum frequency effect) and thus fluoresce more at the higher energy. It is true that in this system, a species absorbing a higher energy photon, e.g., 500 nm, fluoresces at a higher energy, showing a 7.5 nm blueshift from that excited at 540 nm (Figure 6E).

In principle, the IR pulse can do three things to possibly blue-shift the fluorescence: (1) the vibrational relaxation thermalizes and increases the sample temperature, which accelerates the dissociation of dimers to monomers; (2) the IR pulse sums up with the visible pulse to generate ∼497 nm photons as the result of sum-frequency effect (∼1580 cm^{-1} + 540 nm ∼ = 497 nm), which can blue-shift fluorescence if the emission wavelength shows excitation-wavelength dependence; (3) the IR pulse excitons result in some long-lived vibrations and processes comparable to fluorescence lifetime to impact the emission wavelength as well as the line width.

The first possibility is excluded by the temperature-dependent fluorescence spectra displayed in Figure 6D, in which the fluorescence peak red-shifts as temperature increases from 302 to 317 K, opposite to the blueshift observed in the double excitation experiments. As for the sum-frequency effect, the fluorescence also blue-shifts when excited by visible photons with a shorter wavelength (Figure 6E), e.g., the blueshift is 7.5 nm for excitation at 500 nm compared to that excited at 540 nm. In the experiments, only 2 subensembles, monomer and dimer (∼4%, since ∼8% of monomer aggregates), exist in the 0.01 M sample. According to Kasha's[68] rule, the emission spectra excited by any wavelength is the linear combination of the emission spectrum from each species if vibrational relaxations are much faster than the electronic relaxations. Based on this principle, the fluorescence spectra excited by various wavelengths are simulated with the linear combinations of emission spectra excited by 500 nm (monomer-preference) and 540 nm (dimer-preference). The emission spectra excited by 510, 520, and 530 nm can be well described by this method (Figure S9B−D). The simulation also works excellently for the emission spectrum of visible/IR double excitation, nicely reproducing the blue-shifted and broadened line width (Figure 6F).

In a ten-time diluted sample (10^{-3} M), the fluorescence enhancement (3.5 times, Figure S10E) by IR excitation is even larger than in the concentrated sample (2.6 times), but the amplitudes of blueshift and line width broadening are smaller (Figure S10F). According to the principle of equilibrium, the dimer concentration in the diluted solution is only ∼1% (<0.05%) of that (4%) in the concentrated sample. It is therefore that the blueshift and line width broadening observed in the concentrated sample must be partially contributed by the preferential excitation of monomer by the double-excitation, and the fluorescence enhancement must mainly come from the enhancement of the Franck−Condon factor rather than preferential excitation of monomer, which is further supported by the visible photonic energy-dependent double excitation experiments (Figure S9). When the visible photon is close to the electronic resonance center, the sum frequency of it and the IR photon lies on its blue side, which must result in a decrease instead of increase of fluorescence if the Franck−Condon factor altered by vibrational excitation is the main cause. As displayed in Figure S9A showing the visible photonic energy dependence, the double excitation with 500 nm and 1580 cm^{-1} leads to a fluorescence intensity drop compared to that excited with only 500 nm. The results again clearly demonstrate that the change of the Franck−Condon factor is the key for the observed fluorescence change.

The third possibility, long-lived vibrations of low frequencies and processes induced by initiated IR excitations, also plays roles. It is very conceivable that the blue-shifted and broadened fluorescence in the double resonance experiments is also partly because the emission is from higher vibrational excited states, which are the excitations of low-frequency modes coupled to the skeleton stretch rather than the vibrational ground state of the electronic excited state. Previous sub-ps fluorescence experiments have also shown that the emission from the vibrational excited states of the electronic excited state back to the electronic ground state results in a blue-shifted and wider fluorescence.[69−71] To influence the emission wavelength of fluorescence, the lifetimes of the vibrational excited states of the electronic excited state should be much longer than a few ps. They must be comparable to that of the electronic excited state (Figure S4), at least hundreds of ps to a few ns. It is also possible that the initial IR excitation may relax to excite the breathing mode of the dimer molecules, whose lifetime is hundreds of picoseconds to several ns. The excitation of the breathing mode separates two moieties of a dimer, similar to heat-induced dissociation, resulting in the luminescence looking like monomers. In addition, it is also possible that some dimers dissociate due to vibrational relaxations.

This conjecture is confirmed by IR pump/probe experiments. As displayed in Figure S11A, the vibrational excitation signal has a fast decay of about 4.4 ps and a very slow decay of 2.3 ns. The fast component is the decay of strong skeleton stretch vibrational excitation. The long tail is the local "thermal effect" which is caused by the long-lived processes and the solvent heating effect, plus a possible global cooling. The IR pump/IR probe experiments (Figure S11) with various pump and various probe frequencies indicate that probably all the three factors are responsible for the long bleaching tail with the long-lived processes contributing significantly. Similar long tails caused by relaxations of high-frequency vibrations have been previously observed in many other systems.[46,72−74] The

https://doi.org/10.1021/acs.jpca.3c07060
J. Phys. Chem. A 2024, 128, 2912−2922

existence of long-lived processes is further confirmed by the time-delay double-excitation fluorescence enhancement experiments. Fluorescence enhancements in both 10^{-3} and 0.01 M are observed at a very long delay time (IR excitation is 0.8 ns prior to the visible excitation) in Figure S12.

Tentative thoughts about the long-lived vibrations that contribute to fluorescence enhancement are presented in the following. At room temperature, the solvent has many resonant energy acceptors for these modes to dissipate energy. According to the intermolecular dephasing energy transfer theory,[75,76] the coupling strength between some of these modes and the energy acceptors for the transfer must be extremely small to make relaxation slower than a nanosecond (Supporting Information Part 16). In other words, the transition dipole moments of these modes are very small. They are likely more Raman-active than IR-active, and they probably acquire energy from the high-energy modes through mechanical coupling. There is an alternative explanation. The local heat effect generated in the solvent by the vibrational relaxations has not been thermalized within a few ns (Figure S11A). It is possible that some hot solvent modes in the same frequency range are under fast energy exchange equilibrium with these modes of fluorescein, which makes them long-lived. Further investigations are needed to distinguish these possibilities.

3. CONCLUSIONS

In summary, simultaneous intensity enhancement, peak blueshift, and line width broadening of fluorescence are observed in visible/IR double resonance experiments of methanol solutions of fluorescein dianion. By scanning the vibrational excitation frequencies, tuning the time delay between the two excitation pulses, theoretical calculations, and nonlinear and linear spectroscopic measurements, the fluorescence intensity enhancement is mainly attributed to the Franck−Condon factor increased by vibrational excitations at the electron ground state. The relaxations of vibrations initially excited by the IR photons populate the intermediate vibrational modes that may have better enhancement effects. As delay time evolves, the changing distribution of modulation-effective dark modes results in the oscillation of intensity decay, and the varying enhancement effects originating from different vibrations overlap to cause the shifts of effective modulation wavenumbers. The peak blue-shift and line width broadening are caused by both preferentially increasing the Franck−Condon factors among different subensembles with IR pre-excitation and long-lived processes induced by the initial IR excitation. The results also demonstrate that the fluorescence from the visible/IR double resonance experiments is not a simple sum frequency effect or heat effect. The dynamics caused by the vibrational relaxations can introduce profound effects into the fluorescence.

■ ASSOCIATED CONTENT

Supporting Information

The Supporting Information is available free of charge at https://pubs.acs.org/doi/10.1021/acs.jpca.3c07060.

Materials and methods; experimental setup; IR spectra and mode assignments by theoretical calculation; theoretical calculation results of electronic excited state; supplementary notes for fluorescence emission wavelength and line width; fluorescence lifetime; two-dimensional infrared spectra; visible absorption differential spectra with and without infrared modulation; dynamics of vibrational mode-selective fluorescence enhancement of excited fluorescein manipulation; no modulation effect emerges on electronic excited state; estimation of the number of visible-excited molecules; overlapping of the emission spectra with different excitation wavelengths; experimental results with dilute solutions; long-tail in IR pump/IR probe signal decay; dynamics of fluorescence enhancement at long delay time; and dephasing energy transfer theorem and possible Raman-active vibrational modes (PDF)

■ AUTHOR INFORMATION

Corresponding Authors

Jianxin Guan − *College of Chemistry and Molecular Engineering, Beijing National Laboratory for Molecular Sciences, Peking University, Beijing 100871, China*; Email: guanjianxin1125@pku.edu.cn

Junrong Zheng − *College of Chemistry and Molecular Engineering, Beijing National Laboratory for Molecular Sciences, Peking University, Beijing 100871, China*; orcid.org/0000-0002-4472-8576; Email: junrong@pku.edu.cn, zhengjunrong@gmail.com

Authors

Qirui Yu − *College of Chemistry and Molecular Engineering, Beijing National Laboratory for Molecular Sciences, Peking University, Beijing 100871, China*

Xinmao Li − *College of Chemistry and Molecular Engineering, Beijing National Laboratory for Molecular Sciences, Peking University, Beijing 100871, China*

Chengzhen Shen − *College of Chemistry and Molecular Engineering, Beijing National Laboratory for Molecular Sciences, Peking University, Beijing 100871, China*

Zhihao Yu − *College of Chemistry and Molecular Engineering, Beijing National Laboratory for Molecular Sciences, Peking University, Beijing 100871, China*

Complete contact information is available at: https://pubs.acs.org/10.1021/acs.jpca.3c07060

Author Contributions

Q.Y., J.G., and J.Z. designed experiments. J.Z. and J.G. supervised the project. Q.Y. prepared materials and performed spectroscopy experiments. Q.Y., X.L., J.G., and Z.Y. performed ultrafast experiments. Q.Y., X.L., J.G., Z.Y., and J.Z. analyzed data. Q.Y. and C.S. conducted theoretical calculations. Q.Y., J.G., and J.Z. prepared and revised the manuscript.

Notes

The authors declare no competing financial interest.

■ ACKNOWLEDGMENTS

This material is based upon work supported by the National Science Foundation of China (NSFC-22203006, 21927901, 92261206, 21627805, 12174012, 21673004, 21821004, 21674001, and 21790363), MOST (a special talent program) China, and the Beijing City. We also thank the support from the High-performance Computing Platform of Peking University for the computational resources.

REFERENCES

(1) Hochstrasser, R. M. The Luminescence of Organic Molecular Crystals. *Rev. Mod. Phys.* **1962**, *34*, 531−550.
(2) Sagara, Y.; Kato, T. Mechanically induced luminescence changes in molecular assemblies. *Nat. Chem.* **2009**, *1*, 605−610.
(3) Xu, J.; Tanabe, S. Persistent luminescence instead of phosphorescence: History, mechanism, and perspective. *J. Lumin.* **2019**, *205*, 581−620.
(4) Gierschner, J.; Shi, J.; Milián-Medina, B.; Roca-Sanjuán, D.; Varghese, S.; Park, S. Luminescence in Crystalline Organic Materials: From Molecules to Molecular Solids. *Adv. Opt. Mater.* **2021**, *9*, 2002251.
(5) Wang, Y.; Li, X.; Zhao, S.; Wang, B.; Song, X.; Xiao, J.; Lan, M. Synthesis strategies, luminescence mechanisms, and biomedical applications of near-infrared fluorescent carbon dots. *Coord. Chem. Rev.* **2022**, *470*, 214703.
(6) Dhbaibi, K.; Abella, L.; Meunier-Della-Gatta, S.; Roisnel, T.; Vanthuyne, N.; Jamoussi, B.; Pieters, G.; Racine, B.; Quesnel, E.; Autschbach, J.; et al. Achieving high circularly polarized luminescence with push-pull helicenic systems: from rationalized design to top-emission CP-OLED applications. *Chem. Sci.* **2021**, *12*, 5522−5533.
(7) Li, X.-Y.; Shi, W.-J.; Wang, X.-Q.; Ma, L.-N.; Hou, L.; Wang, Y.-Y. Luminescence Modulation, White Light Emission, and Energy Transfer in a Family of Lanthanide Metal-Organic Frameworks Based on a Planar π-Conjugated Ligand. *Cryst. Growth Des.* **2017**, *17*, 4217−4224.
(8) Nicolet, O.; Banerji, N.; Pages, S.; Vauthey, E. Effect of the excitation wavelength on the ultrafast charge recombination dynamics of donor- acceptor complexes in polar solvents. *J. Phys. Chem. A* **2005**, *109*, 8236−8245.
(9) Qi, Q.; Li, C.; Liu, X.; Jiang, S.; Xu, Z.; Lee, R.; Zhu, M.; Xu, B.; Tian, W. Solid-State Photoinduced Luminescence Switch for Advanced Anticounterfeiting and Super-Resolution Imaging Applications. *J. Am. Chem. Soc.* **2017**, *139*, 16036−16039.
(10) Scherbovich, A. A.; Maskevich, S. A.; Karpach, P. V.; Vasilyuk, G. T.; Stsiapura, V. I.; Venidiktova, O. V.; Ayt, A. O.; Barachevsky, V. A.; Khuzin, A. A.; Tuktarov, A. R.; et al. Reversible Photoinduced Luminescence Modulation from Nanospheres Containing CdSe/ZnS Quantum Dots and Photochromic Diarylethene. *J. Phys. Chem. C* **2020**, *124*, 27064−27070.
(11) Zhang, Q.; Zheng, X.; Sun, H.; Li, W.; Wang, X.; Hao, X.; An, S. Dual-Mode Luminescence Modulation upon Visible-Light-Driven Photochromism with High Contrast for Inorganic Luminescence Ferroelectrics. *ACS Appl. Mater. Interfaces* **2016**, *8*, 4789−4794.
(12) Urano, Y.; Kamiya, M.; Kanda, K.; Ueno, T.; Hirose, K.; Nagano, T. Evolution of fluorescein as a platform for finely tunable fluorescence probes. *J. Am. Chem. Soc.* **2005**, *127*, 4888−4894.
(13) Ueno, T.; Urano, Y.; Setsukinai, K.-i.; Takakusa, H.; Kojima, H.; Kikuchi, K.; Ohkubo, K.; Fukuzumi, S.; Nagano, T. Rational principles for modulating fluorescence properties of fluorescein. *J. Am. Chem. Soc.* **2004**, *126*, 14079−14085.
(14) Ma, Z.; Yang, Z.; Mu, L.; Deng, L.; Chen, L.; Wang, B.; Qiao, X.; Hu, D.; Yang, B.; Ma, D.; et al. Converting molecular luminescence to ultralong room-temperature phosphorescence via the excited state modulation of sulfone-containing heteroaromatics. *Chem. Sci.* **2021**, *12*, 14808−14814.
(15) Hu, S.; Yao, Z.; Ma, X.; Yue, L.; Chen, L.; Liu, R.; Wang, P.; Li, H.; Zhang, S.-T.; Yao, D.; et al. Pressure-Induced Local Excitation Promotion: New Route toward High-Efficiency Aggregate Emission Based on Multimer Excited State Modulation. *J. Phys. Chem. Lett.* **2022**, *13*, 1290−1299.
(16) Munch, M.; Colombain, E.; Stoerkler, T.; Vérité, P. M.; Jacquemin, D.; Ulrich, G.; Massue, J. Blue-emitting 2-(2′-Hydroxyphenyl) benzazole fluorophores by modulation of excited-state intramolecular proton transfer: Spectroscopic studies and theoretical calculations. *J. Phys. Chem. B* **2022**, *126*, 2108−2118.
(17) Sjöback, R.; Nygren, J.; Kubista, M. Absorption and fluorescence properties of fluorescein. *Spectrochim. Acta, Part A* **1995**, *51*, 7−21.
(18) Tomasulo, M.; Yildiz, I.; Raymo, F. M. Luminescence modulation with semiconductor quantum dots and photochromic ligands. *Aust. J. Chem.* **2006**, *59*, 175−178.
(19) Lei, Y.; Dai, W.; Guan, J.; Guo, S.; Ren, F.; Zhou, Y.; Shi, J.; Tong, B.; Cai, Z.; Zheng, J.; et al. Wide-Range Color-Tunable Organic Phosphorescence Materials for Printable and Writable Security Inks. *Angew. Chem., Int. Ed.* **2020**, *59*, 16054−16060.
(20) Zhang, Y.; Luo, L.; Li, K.; Li, W.; Hou, Y. Reversible up-conversion luminescence modulation based on UV-VIS light-controlled photochromism in Er 3+ doped Sr 2 SnO 4. *J. Mater. Chem. C* **2018**, *6*, 13148−13156.
(21) John, J.; Thomas, L.; Kurian, A.; George, S. D. Modulating fluorescence quantum yield of highly concentrated fluorescein using differently shaped green synthesized gold nanoparticles. *J. Lumin.* **2016**, *172*, 39−46.
(22) Schmidt, G. C. Beiträge zur Kenntniss der Fluorescenz. *Ann. Phys.* **1896**, *294*, 103−130.
(23) Schmidt, G. C. Über Lumineszenz von festen Lösungen. *Ann. Phys.* **1921**, *370*, 247−256.
(24) Stark, J.; Lipp, P. The effect of inner molecular relative movement on the intensity of absorption of fluorescent by valence electrons. *Z. Phys. Chem.* **1913**, *86*, 36−41.
(25) Guan, J.; Shen, C.; Peng, J.; Zheng, J. What Leads to Aggregation-Induced Emission? *J. Phys. Chem. Lett.* **2021**, *12*, 4218−4226.
(26) Callis, P. R. Two-photon-induced fluorescence. *Annu. Rev. Phys. Chem.* **1997**, *48*, 271−297.
(27) Denk, W.; Strickler, J. H.; Webb, W. W. Two-photon laser scanning fluorescence microscopy. *Science* **1990**, *248*, 73−76.
(28) Letokhov, V. S. Use of Lasers to Control Selective Chemical Reactions. *Science* **1973**, *180*, 451−458.
(29) Ronn, A. M. Infrared Laser Catalyzed Chemical Reactions. *Spectrosc. Lett.* **1975**, *8*, 303−328.
(30) Kurylo, M. J.; Braun, W.; Xuan, C. N.; Kaldor, A. Infrared laser enhanced reactions: Temperature resolution of the chemical dynamics of the O3† + NO reaction systen. *J. Chem. Phys.* **1975**, *62*, 2065−2071.
(31) Langsam, Y.; Ronn, A. M. The Kinetics and Mechanism of Dissociation of Metal-Carbonyls in High Infrared-Laser Fields. *Chem. Phys.* **1981**, *54*, 277−290.
(32) Majima, T.; Ishii, T.; Matsumoto, Y.; Takami, M. Sulfur hexafluoride sensitized infrared photodecomposition of iron pentacarbonyl. *J. Am. Chem. Soc.* **1989**, *111*, 2417−2422.
(33) Utz, A. L. Mode selective chemistry at surfaces. *Curr. Opin. Solid State Mater. Sci.* **2009**, *13*, 4−12.
(34) Heyne, K.; Kühn, O. Infrared laser excitation controlled reaction acceleration in the electronic ground state. *J. Am. Chem. Soc.* **2019**, *141*, 11730−11738.
(35) Levis, R. J.; Menkir, G. M.; Rabitz, H. Selective bond dissociation and rearrangement with optimally tailored, strong-field laser pulses. *Science* **2001**, *292*, 709−713.
(36) Amstrup, B.; Carlson, R. J.; Matro, A.; Rice, S. A. Use of pulse shaping to control the photodissociation of a diatomic molecule: preventing the best from being the enemy of the good. *J. Phys. Chem.* **1991**, *95*, 8019−8027.
(37) Assion, A.; Baumert, T.; Bergt, M.; Brixner, T.; Kiefer, B.; Seyfried, V.; Strehle, M.; Gerber, G. Control of chemical reactions by feedback-optimized phase-shaped femtosecond laser pulses. *Science* **1998**, *282*, 919−922.
(38) Kawashima, H.; Wefers, M. M.; Nelson, K. A. Femtosecond pulse shaping, multiple-pulse spectroscopy, and optical control. *Annu. Rev. Phys. Chem.* **1995**, *46*, 627−656.
(39) Shapiro, M.; Brumer, P. On the origin of pulse shaping control of molecular dynamics. *J. Phys. Chem. A* **2001**, *105*, 2897−2902.
(40) Stensitzki, T.; Yang, Y.; Kozich, V.; Ahmed, A. A.; Kössl, F.; Kühn, O.; Heyne, K. Acceleration of a ground-state reaction by selective femtosecond-infrared-laser-pulse excitation. *Nat. Chem.* **2018**, *10*, 126−131.

https://doi.org/10.1021/acs.jpca.3c07060
J. Phys. Chem. A 2024, 128, 2912−2922

(41) Lin, Z.; Lawrence, C. M.; Xiao, D.; Kireev, V. V.; Skourtis, S. S.; Sessler, J. L.; Beratan, D. N.; Rubtsov, I. V. Modulating unimolecular charge transfer by exciting bridge vibrations. *J. Am. Chem. Soc.* **2009**, *131*, 18060−18062.
(42) Whaley-Mayda, L.; Guha, A.; Penwell, S. B.; Tokmakoff, A. Fluorescence-Encoded Infrared Vibrational Spectroscopy with Single-Molecule Sensitivity. *J. Am. Chem. Soc.* **2021**, *143*, 3060−3064.
(43) Wang, H.; Lee, D.; Cao, Y.; Bi, X.; Du, J.; Miao, K.; Wei, L. Bond-selective fluorescence imaging with single-molecule sensitivity. *Nat. Photonics* **2023**, *17*, 846−855.
(44) Crim, F. F. Bond-selected chemistry: vibrational state control of photodissociation and bimolecular reaction. *J. Phys. Chem.* **1996**, *100*, 12725−12734.
(45) Crim, F. F. Chemical dynamics of vibrationally excited molecules: Controlling reactions in gases and on surfaces. *Proc. Natl. Acad. Sci. U.S.A.* **2008**, *105*, 12654−12661.
(46) Rubtsov, I. V. Relaxation-assisted two-dimensional infrared (RA 2DIR) method: Accessing distances over 10 Å and measuring bond connectivity patterns. *Acc. Chem. Res.* **2009**, *42*, 1385−1394.
(47) Rubtsov, I. V.; Wang, J.; Hochstrasser, R. M. Dual-frequency 2D-IR spectroscopy heterodyned photon echo of the peptide bond. *Proc. Natl. Acad. Sci. U.S.A.* **2003**, *100*, 5601−5606.
(48) Delor, M.; Archer, S. A.; Keane, T.; Meijer, A. J. H. M.; Sazanovich, I. V.; Greetham, G. M.; Towrie, M.; Weinstein, J. A. Directing the path of light-induced electron transfer at a molecular fork using vibrational excitation. *Nat. Chem.* **2017**, *9*, 1099−1104.
(49) Delor, M.; Keane, T.; Scattergood, P. A.; Sazanovich, I. V.; Greetham, G. M.; Towrie, M.; Meijer, A. J. H. M.; Weinstein, J. A. On the mechanism of vibrational control of light-induced charge transfer in donor-bridge-acceptor assemblies. *Nat. Chem.* **2015**, *7*, 689−695.
(50) Delor, M.; Scattergood, P. A.; Sazanovich, I. V.; Parker, A. W.; Greetham, G. M.; Meijer, A. J.; Towrie, M.; Weinstein, J. A. Toward control of electron transfer in donor-acceptor molecules by bond-specific infrared excitation. *Science* **2014**, *346*, 1492−1495.
(51) Huang, Y.; Rettner, C. T.; Auerbach, D. J.; Wodtke, A. M. Vibrational promotion of electron transfer. *Science* **2000**, *290*, 111−114.
(52) Bredenbeck, J.; Helbing, J.; Hamm, P. Labeling vibrations by light: Ultrafast transient 2D-IR spectroscopy tracks vibrational modes during photoinduced charge transfer. *J. Am. Chem. Soc.* **2004**, *126*, 990−991.
(53) Hamm, P. Coherent effects in femtosecond infrared spectroscopy. *Chem. Phys.* **1995**, *200*, 415−429.
(54) Biasin, E.; Fox, Z. W.; Andersen, A.; Ledbetter, K.; Kjær, K. S.; Alonso-Mori, R.; Carlstad, J. M.; Chollet, M.; Gaynor, J. D.; Glownia, J. M.; et al. Direct observation of coherent femtosecond solvent reorganization coupled to intramolecular electron transfer. *Nat. Chem.* **2021**, *13*, 343−349.
(55) Courtney, T. L.; Fox, Z. W.; Slenkamp, K. M.; Khalil, M. Two-dimensional vibrational-electronic spectroscopy. *J. Chem. Phys.* **2015**, *143*, 154201.
(56) Kern-Michler, D.; Neumann, C.; Mielke, N.; van Wilderen, L. J. G. W.; Reinfelds, M.; von Cosel, J.; Santoro, F.; Heckel, A.; Burghardt, I.; Bredenbeck, J. Controlling Photochemistry via Isotopomers and IR Pre-excitation. *J. Am. Chem. Soc.* **2018**, *140*, 926−931.
(57) von Cosel, J.; Cerezo, J.; Kern-Michler, D.; Neumann, C.; van Wilderen, L. J. G. W.; Bredenbeck, J.; Santoro, F.; Burghardt, I. Vibrationally resolved electronic spectra including vibrational pre-excitation: Theory and application to VIPER spectroscopy. *J. Chem. Phys.* **2017**, *147*, 164116.
(58) Lin, Z.; Rubtsov, I. V. Constant-speed vibrational signaling along polyethyleneglycol chain up to 60-Å distance. *Proc. Natl. Acad. Sci. U.S.A.* **2012**, *109*, 1413−1418.
(59) Arbeloa, I. L. Dimeric and trimeric states of the fluorescein dianion. Part 1.—Molecular structures. *J. Chem. Soc., Faraday Trans. 2* **1981**, *77*, 1725−1733.
(60) Arbeloa, I. L. Dimeric and trimeric states of the fluorescein dianion. Part 2.—Effects on fluorescence characteristics. *J. Chem. Soc., Faraday Trans. 2* **1981**, *77*, 1735−1742.
(61) Valdes-Aguilera, O.; Neckers, D. Aggregation phenomena in xanthene dyes. *Acc. Chem. Res.* **1989**, *22*, 171−177.
(62) Guan, J.; Wei, R.; Prlj, A.; Peng, J.; Lin, K. H.; Liu, J.; Han, H.; Corminboeuf, C.; Zhao, D.; Yu, Z.; et al. Direct Observation of Aggregation-Induced Emission Mechanism. *Angew. Chem.* **2020**, *132*, 15013−15019.
(63) Chen, H.; Bian, H.; Li, J.; Wen, X.; Zheng, J. Ultrafast multiple-mode multiple-dimensional vibrational spectroscopy. *Int. Rev. Phys. Chem.* **2012**, *31*, 469−565.
(64) Deàk, J. C.; Rhea, S. T.; Iwaki, L. K.; Dlott, D. D. Vibrational energy relaxation and spectral diffusion in water and deuterated water. *J. Phys. Chem. A* **2000**, *104*, 4866−4875.
(65) Iwaki, L. K.; Dlott, D. D. Three-dimensional spectroscopy of vibrational energy relaxation in liquid methanol. *J. Phys. Chem. A* **2000**, *104*, 9101−9112.
(66) Stuchebrukhov, A. A.; Marcus, R. A. Theoretical study of intramolecular vibrational relaxation of acetylenic CH vibration for v = 1 and 2 in large polyatomic molecules (CX3)3YCCH, where X = H or D and Y = C or Si. *J. Chem. Phys.* **1993**, *98*, 6044−6061.
(67) Cerezo, J.; Santoro, F. FCclasses3: Vibrationally-resolved spectra simulated at the edge of the harmonic approximation. *J. Comput. Chem.* **2023**, *44*, 626−643.
(68) Kasha, M. Characterization of electronic transitions in complex molecules. *Discuss. Faraday Soc.* **1950**, *9*, 14−19.
(69) Mokhtari, A.; Chebira, A.; Chesnoy, J. Subpicosecond fluorescence dynamics of dye molecules. *J. Opt. Soc. Am. B* **1990**, *7*, 1551−1557.
(70) Cannizzo, A.; van Mourik, F.; Gawelda, W.; Zgrablic, G.; Bressler, C.; Chergui, M. Broadband femtosecond fluorescence spectroscopy of [Ru(bpy)3]2+. *Angew. Chem., Int. Ed.* **2006**, *45*, 3174−3176.
(71) Schanz, R.; Kovalenko, S.; Kharlanov, V.; Ernsting, N. Broad-band fluorescence upconversion for femtosecond spectroscopy. *Appl. Phys. Lett.* **2001**, *79*, 566−568.
(72) Bian, H.; Chen, H.; Li, J.; Wen, X.; Zheng, J. Nonresonant and Resonant Mode-Specific Intermolecular Vibrational Energy Transfers in Electrolyte Aqueous Solutions. *J. Phys. Chem. A* **2011**, *115*, 11657−11664.
(73) Bian, H.; Zhao, W.; Zheng, J. Intermolecular vibrational energy exchange directly probed with ultrafast two dimensional infrared spectroscopy. *J. Chem. Phys.* **2009**, *131*, 124501.
(74) Kurochkin, D. V.; Naraharisetty, S. R. G.; Rubtsov, I. V. A relaxation-assisted 2D IR spectroscopy method. *Proc. Natl. Acad. Sci. U.S.A.* **2007**, *104*, 14209−14214.
(75) Chen, H.; Wen, X.; Guo, X.; Zheng, J. Intermolecular vibrational energy transfers in liquids and solids. *Phys. Chem. Chem. Phys.* **2014**, *16*, 13995−14014.
(76) Chen, H.; Bian, H.; Li, J.; Wen, X.; Zhang, Q.; Zhuang, W.; Zheng, J. Vibrational energy transfer: an angstrom molecular ruler in studies of ion pairing and clustering in aqueous solutions. *J. Phys. Chem. B* **2015**, *119*, 4333−4349.

https://doi.org/10.1021/acs.jpca.3c07060
J. Phys. Chem. A 2024, 128, 2912−2922